Is a Hydrophobic Amino Acid Required To Maintain the Reactive V Conformation of Thiamin at the Active Center of Thiamin Diphosphate-Requiring Enzymes? Experimental and Computational Studies of Isoleucine 415 of Yeast Pyruvate Decarboxylase[†]

Fusheng Guo, Deqi Zhang, Ara Kahyaoglu, Ramy S. Farid, and Frank Jordan*

Department of Chemistry and Program in Cellular and Molecular Biodynamics, Rutgers, the State University of New Jersey, Newark, New Jersey 07102

Received March 27, 1998; Revised Manuscript Received June 29, 1998

ABSTRACT: The residue I415 in pyruvate decarboxylase from *Saccharomyces cerevisiae* was substituted with a variety of uncharged side chains of varying steric requirements to test the hypothesis that this residue is responsible for supporting the V coenzyme conformation reported for this enzyme [Arjunan et al. (1996) *J. Mol. Biol. 256*, 590−600]. Changing the isoleucine to valine and threonine decreased the k_{cat} value and shifted the k_{cat}−pH profile to more alkaline values progressively, indicating that the residue at position 415 not only is important for providing the optimal transition state stabilization but also ensures correct alignment of the ionizable groups participating in catalysis. Substitutions to methionine (the residue used in pyruvate oxidase for this purpose) or leucine (the corresponding residue in transketolase) led to greatly diminished k_{cat} values, showing that for each thiamin diphosphate-dependent enzyme an optimal hydrophobic side chain evolved to occupy this key position. Computational studies were carried out on the wild-type enzyme and the I415V, I415G, and I415A variants in both the absence and the presence of pyruvate covalently bound to C2 of the thiazolium ring (the latter is a model for the decarboxylation transition state) to determine whether the size of the side chain is critically required to maintain the V conformation. Briefly, there are sufficient conformational constraints from the binding of the diphosphate side chain and three conserved hydrogen bonds to the 4′-aminopyrimidine ring to enforce the V conformation, even in the absence of a large side chain at position 415. There appears to be increased coenzyme flexibility on substitution of Ile415 to Gly in the absence compared with the presence of bound pyruvate, suggesting that entropy contributes to the rate acceleration. The additional CH_3 group in Ile compared to Val also provides increased hydrophobicity at the active center, likely contributing to the rate acceleration. The computational studies suggest that direct proton transfer to the 4′-imino nitrogen from the thiazolium C2H is eminently plausible.

One of the striking findings revealed by the X-ray crystal structures of enzymes that utilize thiamin diphosphate (ThDP,[1] the vitamin B1 coenzyme) as cofactor, pyruvate decarboxylase (PDC; see Scheme 1 for reaction) from *Saccharomyces uvarum* (*1*) and *Saccharomyces cerevisiae* (*2*), pyruvate oxidase (POX) *from Lactobacillus plantarum* (*3*), and transketolase (TK) from bakers' yeast (*4*) is the unusual V conformation of the cofactor. This description applies to the disposition of the two planar aromatic rings, thiazolium and 4′-amino-2-methylpyrimidine, connected via their N3 and C5′ atoms, respectively, through a bridging methylene group. For many years, in X-ray studies of thiamin and its derivatives predominantly the F (for free) and S (for substituted at the reactive C2 atom) conformers were observed (*5*). These conformations are conveniently described by two torsional angles Φ_T and Φ_P for rotations around the N3−C_{br} and C5′−C_{br} bonds, respectively (for the V conformation $\Phi_T = \pm 90°$ and $\Phi_P \mp 90°$, for the F conformation $\Phi_T = 0$ and $\Phi_P = \pm 90°$, and for the S conformation $\Phi_T = \pm 100$ and $\Phi_P = \pm 150°$). Of more than 60 relevant structures of thiamin analogues studied to date, there were only three instances reported of the V conformation: oxythiamin (*6*), thiamin 2-thiazolone (*7*), and 4′-deaminothiamin (*8*), the first and third of the three lacking the 4′-amino group. Earlier conformational maps employing a potential energy function dominated by nonbonding interactions indicated that the V conformation is energetically unfavorable both for unsubstituted thiamin and for C2-

[†] Supported by NIH GM-50380 (F.J.), NSF Training Grant BIR 94/13198 in Cellular and Molecular Biodynamics [R.S.F. and F.J. (principal investigator)], the Rutgers University Busch Biomedical Fund (R.S.F. and F.J.), and Hoffmann La Roche Diagnostics Inc. Somerville, NJ.

* To whom correspondence should be addressed: Tel 973-353-5470, FAX 973-353-1264; E-mail frjordan@newark.rutgers.edu.

[1] Abbreviations: ThDP, thiamin diphosphate; PDC, pyruvate decarboxylase (E.C. 4.1.1.1); WT, enzyme produced in *Escherichia coli* from the wild-type pdc1 (pyruvate decarboxylase) gene isolated from *Saccharomyces cerevisiae*; I415A, I415T, I415L, I415M, I415V, and I415S, variants at position 415 occupied by isoleucine in the wild-type enzyme; LThDP, 2-(2-lactyl)thiamin diphosphate; SDS−PAGE, sodium dodecyl sulfate−polyacrylamide gel electrophoresis; PCR, polymerase chain reaction; DEAE, diethylaminoethyl; EDTA, ethlenediaminetetraacetic acid; PMSF, phenylmethanesulfonyl fluoride; MES, 2-(*N*-morpholino)ethanesulfonic acid; MOPS, 3-(*N*-morpholino)propanesulfonic acid; NADH, nicotinamide adenine dinucleotide (reduced).

S0006-2960(98)00709-0 CCC: $15.00
Published on Web 08/29/1998

Scheme 1

Thiamin Diphosphate, ThDP **Mechanism of pyruvate decarboxylase, PDC**

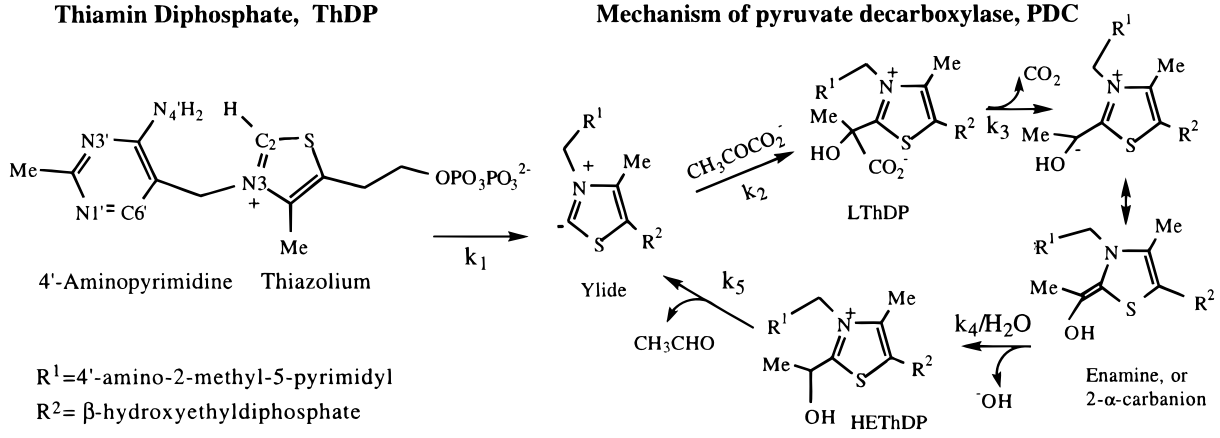

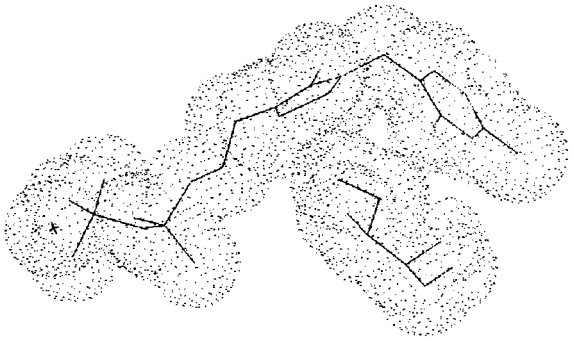

FIGURE 1: van der Waals interactions between I415 and ThDP on PDC.

substituted structures resembling some of the reaction intermediates (*9*, *10*), although a more recent and more complete potential function has made the conformational preferences less pronounced (*11*). On the three enzymes referred to above, the V conformation appears to be supported by the presence of a bulky hydrophobic side chain: isoleucine in PDC (Figure 1), methionine in POX, and leucine in TK, whose side-chain termini are within van der Waals distance of the coenzyme.

In this study we have begun to identify the reasons for this high degree of selection of residue 415 and for the V conformation on all of these enzymes. Herein are reported kinetic properties of the wild-type (WT) PDC compared to those of the I415V, I415T, I415A, I415S, I415L, and I415M variants. The activity of the enzyme is found to progressively diminish with a decrease in the size of group 415. The PDC variants with methionine and leucine substitutions at position 415 were prepared in an attempt to understand why isoleucine was selected for PDC, rather than the methionine found in POX or leucine found in TK at the corresponding positions. In addition, computational studies were conducted using molecular mechanics approaches to estimate the conformational preferences of the variant enzymes with respect to the Φ_T and Φ_P conformational angles.

The combination of steady-state kinetic studies coupled with molecular mechanics calculations of the preferred ThDP conformations in the variants revealed that isoleucine at position 415 is a pivotal residue since it appears to be responsible for imposing optimized hydrogen bonding to the 4′-aminopyrimidine of ThDP. The possibility that I415 participates in the putative substrate activation pathway, triggered at cysteine 221 (*12*−*16*), was also explored.

EXPERIMENTAL PROCEDURES

Materials. The T7 *Escherichia coli* expression system was purchased from Novagen Inc. The *E. coli* DH5α cells and low melting point agarose were from Life Technologies, Inc.; *Pfu* DNA polymerase was from Stratagene. Restriction enzymes, Wizard PCR purification kit, Wizard plasmid miniprep kit, 373 DNA sequencing plasmid prep kit, and dNTPs were from Promega; the DNA sequencing kit was from Perkin-Elmer. LB medium (Difco) was from Fisher Scientific; Sephacryl S300 HR and DEAE-Sephacel were from Pharmacia, and hydroxylapatite (HTP) gel was from Bio-Rad Laboratories.

Site-Directed Mutagenesis. The site-directed mutagenesis experiments were carried out with the PCR megaprimer method (*17*), which needs two universal flanking primers and one mutagenic primer and two subsequent PCR amplifications. Purified pET22b(+)pdc1, containing the entire coding region for the yeast pdc1 gene (PDC1 from *Saccharomyces cerevisiae*), was used as the template in the PCR. Two 26-mer synthetic oligonucleotides, 5′-CCGCGAAATTAATACGACTCACATTA-3′ and 5′-GTTATGCTAGTTATTGCTCGAAGGTC-3′, corresponding to the pET22b(+) vector T7 promoter and T7 terminator, respectively, were used as two universal flanking primers. The six 33-mer synthetic oligonucleotides coding for the indicated substitutions were designed as follows: 5′-CAAGTCTTATGGGGATCCCGTGGTTTCACCACT-3′ for I415V; 5′-CAAGTCTTATGGGGATCCGCTGGTTTCACCACT-3′ for I415A; 5′-CAAGTCTTATGGGGATCCACTGGTTTCACCACT-3′ for I415T; 5′-CAAGTCTTATGGGGATCCATGGGTTTCACCACT-3′ for I415M; 5′-CAAGTCTTATGGGGATCCCTTGGTTTCACCACT-3′ for I415L and 5′-CAAGTCTTATGGGGATCCAGTGGTTTCACCACT-3′ for I415S. In the first PCR amplification, each of the above mutagenic primers was used together with its antiparallel universal flanking primer 5′-GTTATGCTAGTTATTGCTCGAAGGTC-3′ to yield a PCR fragment that was subsequently used as a megaprimer in the second PCR amplification in conjunction with the other universal flanking primer 5′-CAAGTCTTATGGGGATCCGCTGGTTTCACCACT-3′. The second PCR amplified fragment was cloned into the pET22b(+) vector at the *Xba*I/*Sac*I sites. The resulting

recombinant vectors were transformed into *E. coli* DH5α strain. The mutated constructs were confirmed by DNA sequencing using an Applied Biosystems 373 DNA sequencer. The desired mutant plasmids were further transformed into competent *E. coli* BL21(DE3) strain for protein overexpression.

Expression and Purification of Wild-Type and Variant PDCs in E. coli. *E. coli* BL21(DE3) harboring pET22b-(+)pdc1 was grown at 37 °C with shaking in LB medium containing 50 μg/mL ampicillin. PDC expression was induced by adding 1.0 mM isopropyl β-D-thiogalactopyranoside (IPTG, Promega) to the cell culture in the late-exponential growth phase and the culture was then incubated for an additional 3 h. The cell pellet harvested from 1 L of culture was suspended in about 30 mL of 20 mM phosphate buffer, pH 7.0, containing 2 mM ThDP, 2 mM $MgCl_2$, 1 mM EDTA, 1 mM PMSF, and 2 mM β-mercaptoethanol. The cell extracts, prepared through sonication, were subjected to heat treatment at 50 °C for 10 min. The cell debris was removed by centrifugation. The WT PDC was purified by gradient elution through a DEAE-Sephacryl anion-exchange column followed by a hydroxylapatite column. Buffer A for the DEAE column was 50 mM phosphate (pH 6.8), and buffer B was 250 mM phosphate (pH 5.5). Buffer A for the HTP column was 50 mM phosphate (pH 6.8); buffer B was the same as buffer A but also contained 0.1 mM $CaCl_2$ and 100 mM NaCl. The variant PDC proteins were purified by chromatography on a Sephacyl S300 gel-filtration column and in some cases on the DEAE column, eluting with 50 mM MES (pH 6.0). All elution buffers contained ThDP (1 mM), $MgCl_2$ (1 mM), EDTA (0.1 mM), PMSF (0.1 mM), and 2-mercaptoethanol (1 mM). SDS−PAGE analysis was carried out to check the purity of the preparations.

Enzyme Assay and Kinetic Studies. Protein content was determined according to Bradford (*18*), using the Bio-Rad reagent with bovine serum albumin as standard. Enzyme activity was assayed by the alcohol dehydrogenase- (ADH-) coupled assay by monitoring the depletion of NADH with time at 340 nm (*19*) at 25 °C. A Cobas-Bio centrifugal UV−visible analyzer (Roche Diagnostics) was also used to generate steady-state kinetic data at different pH values, and the slope of the linear region of the absorbance versus time curve was used as the initial velocity. The system simultaneously combines 200 μL of reaction buffer (MES, MOPS, and citrate all at 50 mM, Mg(II) and ThDP at 1 mM each, EDTA at 0.1 mM, ADH at 102 units/mL, and β-NADH at 0.25 mM) with 10 μL of pyruvate ranging from 0.02 to 100 mM in 25 vials. The reaction is initiated with addition of 10 μL of PDC (0.2−0.5 unit). Total volume of the reaction mix including 20 μL flushing volume after addition of substrate and protein was 240 μL. The instrument can assay 24 samples simultaneously.

The kinetic data were fitted to the Hill equation: $v_0/E_0 = (k_{cat}S^n)/\{(S_{0.5})^n + S^n(1 + [I]/K_i)\}$ and the parameters were determined from a linear least-squares fit using the DeltaGraphPro4 program from DeltaPoint Inc. (Monterey, CA).

The data were also treated according to the mechanism in Scheme 2, upper left, specific to PDC, and assuming two pyruvate sites, one regulatory and one catalytic, as developed by Schowen and collaborators (*20*):

$$v_0 = V_{max}\, S^2/\{A + BS + S^2(1 + ([S]/K_i))\} \qquad (1)$$

from which instead of the conventional V_{max}, K_m, and V_{max}/K_m (for the current case, V_{max}, $S_{0.5}$, and $V_{max}/S_{0.5}$), the constants V_{max}, V_{max}/B, or V_{max}/A (and, if accurate enzyme concentrations are known, k_{cat}, k_{cat}/B, and k_{cat}/A) corresponding to a collection of rate constants zero, first, and second order in S, respectively, are obtained. These composite rate constants are plotted against pH so that mechanistic interpretations can be deduced for the function of the variants. It is also relevant (see below) that while in the WT PDC the substrate inhibition is modest, in some of the variants it is quite pronounced, hence its explicit inclusion in the kinetic treatments is required at all pH values.

The errors in the tables were estimated by using a rearranged form of eq 1 with the Kaleidagraph software (Synergy Software, Reading, PA).

pK_{app} values were determined from log (kinetic constant) vs pH plots (when the quality of the data permitted), assuming a Dixon−Webb scheme for protonic equilibria (*21*).

THEORETICAL CALCULATIONS

(A) Wild-Type PDC and I415V, I415A, and I415G Variants. The molecular modeling software package Sybyl 6.30 by Tripos (St. Louis, MO) was used on an Indigo2 Silicon Graphics workstation for visualization and theoretical calculations (*22*). The X-ray crystal structure of the pyruvate decarboxylase from *Saccharomyces uvarum* (Protein Data Bank filename 1pyd) was used in this study. The Φ_T and Φ_P angles in the monomer of *Saccharomyces uvarum* selected for the conformational studies (the only structure available when this study was undertaken) are within 4° of the values in the corresponding monomer from *Saccharomyces cerevisiae*, well within the standard deviations calculated in the conformational searches (see tables). Residues more than 8 Å from the thiamin diphosphate cofactor were ignored, creating a spherical subset of 75 residues. This assured that at least one layer of residues in contact with the cofactor was included in the energy calculations. Hydrogen atoms were added using the Biopolymer:Add Hydrogen algorithm within the Sybyl software. Hydroxyl proton rotamers were manually adjusted to avoid unfavorable contacts while optimizing any potential hydrogen bonds to proton acceptors. To relax strain from crystal packing forces and from the addition of hydrogen atoms, the 8 Å subset of residues including the cofactor were minimized for only 5 iterations using the Tripos force field, Pullman charges, and the conjugate gradient minimization algorithm. The minimized subset of residues has a root mean square (RMS) deviation from the X-ray structure of <0.13 Å for all non-hydrogen atoms, indicating little change in the structure upon minimization, as expected.

Systematic searches of all rotatable single bonds within the cofactor and the residue at position 415 were carried out with the minimized 8 Å subset of residues. The Pα atom of ThDP and the main-chain Cα atom of I415 were used as anchors. The energy of every rotamer was calculated by using the Tripos force field; structures within a 20 kcal/mol energy window were stored for subsequent analysis. Three separate runs were conducted: the first one ignored electrostatics to probe the effect of hydrophobic interactions

Scheme 2: Details and Possible Proton Transfer Steps in the Mechanism of PDC

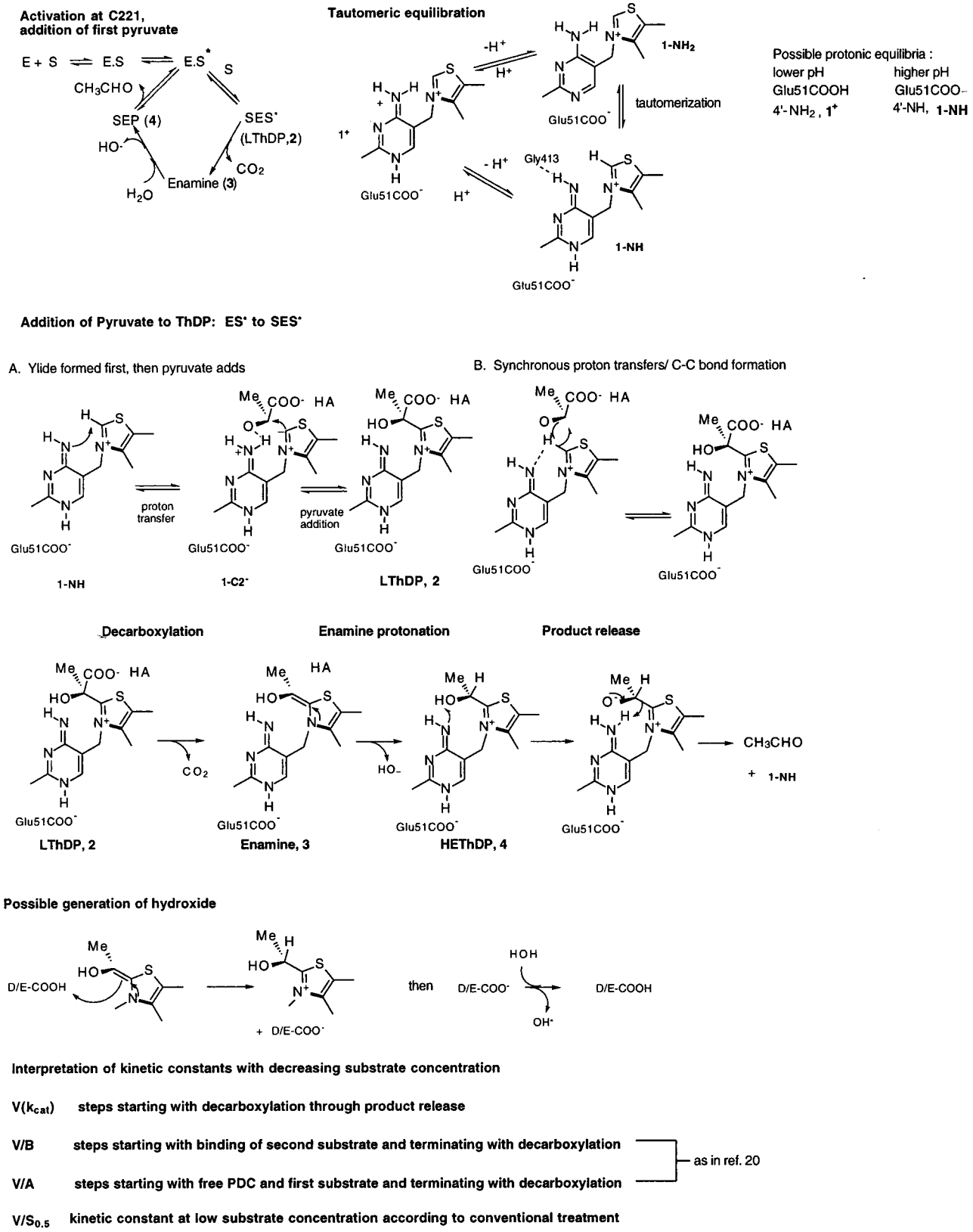

alone; the second included electrostatics (Pullman charges, which assign a positive charge to the sulfur and slightly negative charge to the nitrogen of the thiazolium ring) and used a dielectric constant of 6 to mimic the effect of a nonpolar environment; the third also included electrostatics but used a dielectric constant of 80 to mimic the effect of a highly polar environment.

(B) Calculations on 2-(2-Lactyl)-ThDP Bound to WT PDC and Variants. 2-(2-Lactyl)-ThDP (LThDP) is the first covalent intermediate formed between ThDP and pyruvate; it is the complex that undergoes decarboxylation according to the Breslow mechanism (*23*), and sterically it resembles the transition state for decarboxylation. This complex was modeled by considering both enantiomers and conducting a

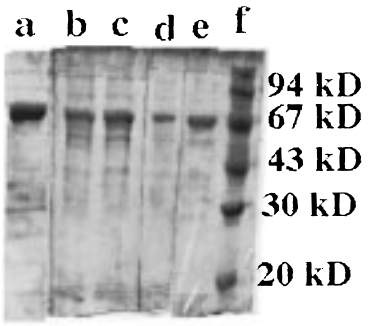

FIGURE 2: SDS−PAGE of WT and variant PDCs. Lane a, WT PDC purified by consecutive chromatography on DEAE and HTP matrixes; lane b, I415V; lane c, I415T; lane d, I415A; lane e, I415M. Lane f shows the position of molecular mass markers (Pharmacia): phosphorylase, 94 kDa; bovine serum albumin, 67 kDa; ovalbumin, 43 kDa; carbonic anydrase, 30 kDa; soybean trypsin inhibitor, 20 kDa. All variant enzymes were purified on Sephacryl S300 HR (Pharmacia).

systematic search of all rotatable bonds. The following potential hydrogen-bonding distances were monitored in the systematic searches: *D*1, I415N−H···N3′; *D*2, E51C═O···H−N1′; *D*3, G413C═O···H−N4′; and *D*4, N4′···C2 or N4′···C2−H.

The conformational searches were carried out on two different tautomeric forms of the 4′-aminopyrimidine ring: the amino tautomer (two hydrogens at the 4′-nitrogen, coplanar with the pyrimidine ring) and imino tautomer (the hydrogen retained at the 4′-nitrogen is hydrogen-bonded to the G413 main-chain carbonyl oxygen, a hydrogen bond that is conserved in all ThDP enzymes). In a recent paper (*2*) it was argued that it is difficult to fit both amino hydrogens along with the thiazolium C2H into the space allowed by the V conformation. This deduction was made in light of our earlier studies of chemical models, indicating that in the N1′-protonated form of the pyrimidine ring the amino group would be strongly conjugated and coplanar with the pyrimidine ring, thereby limiting the allowable conformational space (*24*).

RESULTS

Kinetic Studies of I415 Variants

Preparation and Purification of the Variants. The I415L, I415V, I415T, I415M, I415A, and I415S variant PDCs were constructed. The first three were more stable than the others and could be purified to homogeneity. The I415M, I415A, and I415S variants presented major purification problems and were only purified through Sephacryl S-300HR gel filtration. The SDS−PAGE results for the WT and I415 variant PDCs are presented in Figure 2. The WT PDC appeared homogeneous after purification according to a modified version of the method reported by Farrenkopf and Jordan (*25*). The problems encountered with the purification of the variants were common to all active-center variants produced in this laboratory. Unlike the WT and the I415L, I415V, and I415T variants, the remaining variant enzymes became more unstable with each successive purification step. Increasing ThDP concentration (from 1 to 10 mM) did not prevent loss of the activity, suggesting that the loss of activity during the purification procedure was not solely due to impaired ThDP binding. When subjected to Sephacryl S-300HR gel filtration, the overexpressed I415A and I415M variants remained stable and had satisfactory purity with modestly diminished specific activity after this step. The enzymes were stored at −20 °C with 50% glycerol and under these conditions they were stable for months.

Kinetic Consequences of a Systematic Decrease of the Size of the Side Chain at Position 415. The steady-state kinetic constants at different pH values are presented in Figures S1A−E in the Supporting Information. The kinetic constants at pH 6.0, near the optimum for the WT, are summarized in Table 1, and those at different pH values are given in Tables S1−S5 in the Supporting Information.

When comparing WT to the I415V and I415T variants in the entire pH range studied, as the size of the 415 substituent is decreased, $S_{0.5}$ is only slightly changed, but k_{cat} and $k_{cat}/S_{0.5}$ are both diminished. Therefore, I415 has its greatest effect on the heights of transition-state barriers, not on substrate binding. The k_{cat}−pH curve is unambiguously shifted to the alkaline region in the I415V and I415T variants compared to the WT, and there is also an indication that the magnitude of the shift varies inversely with the size of the group. That is, compared to the WT, in the I415V variant the maximum is shifted ca. 0.6 pH unit, while in the I415T variant, the shift is 1.0 pH unit. These observations signal that the precise size of the steric bulk of Ile415 is required to correctly position the ionizable groups responsible for the

Table 1: Kinetic Parameters of WT and PDC Variants at Position 415[a,b]

	at pH 6.0						at the pH optimum for each parameter			
	k_{cat} (s^{-1})	$k_{cat}/S_{0.5}$ (s^{-1} mM^{-1})	k_{cat}/A (s^{-1} mM^{-1})	k_{cat}/B (s^{-1} mM^{-1})	K_I (mM)	n	k_{cat} (s^{-1})	$k_{cat}/S_{0.5}$ (s^{-1} mM^{-1})	k_{cat}/A (s^{-1} mM^{-1})	k_{cat}/B (s^{-1} mM^{-1})
WT	40	30.7	73	82	>1000	1.9	40 (pH 6.2)	35.8 (pH 5.6)	102.1(pH 5.8)	99 (pH 5.8)
	100	100	100	100		100	100	100	100	
I415V	2.4	1.9	3.5	3.2	280	1.5	3.8 (pH 7.0)	1.9 (pH 6.2)	10. (pH 5.4)	3.3 (pH 6.2)
	6.0	6.2	4.8	3.9			9.5	4.8	9.8	3.3
I415T	1.0	0.48	0.39	1.1	197	1.6	3.0 (pH 7.6)	0.48 (pH 6.2)	1.3 (pH 5.4)	1.6 (pH 6.6)
	2.5	1.6	0.53	1.3			7.5	1.3	1.3	1.6
I415A	0.68	0.44	0.28	16	37	2.1	0.86 (pH 7.2)	0.50 (pH 5.6)	0.50 (pH 5.6)	
	1.7	1.4	0.38	19			2.2	1.4	0.5	
I415M	0.31	0.160	0.11	0.96	51	2.0	0.38 (pH 7.4)	0.16 (pH 5.8)	0.16 (pH 5.8)	
	0.78	0.52	0.15	1.2			1.0	0.4	0.16	
I415S	0.57					1.4	0.57 (pH 6.5)			
	1.4						1.4			
I415L	3.3					1.6	3.4 (pH 5.8)			
	8.3						8.4			

[a] Lower figures represent percentage values compared to the WT PDC. [b] Error analysis is provided in Tables S1−S5 in the Supporting Information.

Table 2: pK_{app} of PDC Variants Estimated from pH-Dependent Kinetic Parameters[a]

	WT		I415V		I415T		I415A		I415M	
	pK_{a1}	pK_{a2}	pK_{a1}	pK_{a2}	pK_{a1}	pK_{a2}	pK_{a1}	pK_{a2}	pK_{a1}	pK_{a2}
log (k_{cat})	5.2	>7.0	5.8	>7.2	6.4	>7.5	~6.7	ND	~6.4	ND
log ($k_{cat}/S_{0.5}$)	5.4	6.1	5.2	6.6	5.5	6.7	5.3	6.7	5.4	6.7
log (k_{cat}/A)	5.4	6.0	ND	6.3	ND	ND	5.4	6.0	5.3	6.0
log (k_{cat}/B)	5.4	6.2	5.7	6.5	5.9	6.6	ND	ND	ND	ND
$k_{cat}K_i$	5.5		6.0			6.4				
K_i	5.7		6.2			6.0				

[a] From data in Tables S1−S5 and Figures S1A−E in the Supporting Information. Estimated error ± 0.3−0.5 unit; data in the top row were calculated from log (k_{cat})−pH plots; $k_{cat}/S_{0.5}$−pH, k_{cat}/A−pH, and k_{cat}/B−pH plots were used for data in rows 2−4; pK_{a1} and pK_{a2} refer to the apparent values determined on the acid and alkaline side of the curves, assuming only a single ionizable group on each side; ND, no values could be estimated from the data.

pH dependence of k_{cat}. All of the substitutions in this paper retain a neutral side chain at position 415, introducing only different steric bulk; hence the shifts in the pH-dependent optima are interpretable. These shifts in the pH optima signal that the conjugate acidity of the group(s) responsible for the acidic limb diminishes and the conjugate basicity of the group responsible for the alkaline limb is progressively enhanced with diminishing size of the 415 side chain. It is more difficult to draw conclusions for k_{cat} on the alkaline side of the plots due to the limited pH range available.

The shapes of k_{cat}/A−pH plots (starting with free substrate and enzyme and culminating with the decarboxylation step) and k_{cat}/B−pH plots (starting with the activated form of the enzyme—presumably with regulatory pyruvate molecule already installed at C221—and culminating with the decarboxylation step) are changed little by substitution at position 415. Again, the I415V and I415L offer useful comparisons: there is a modest shift of the maxima of the bell-shaped curve to more alkaline pH with diminishing size of the substituent at position 415.

The pK_as deduced from the kinetic plots are summarized in Table 2.

Interchanging I415 for Corresponding Residues on Other ThDP Enzymes. A different comparison addresses why nature selects different groups for the position corresponding to 415 (the side chain located under the V conformation) in the different enzymes. The k_{cat} is much lower for the leucine than for the isoleucine substituent, ca. 9−10-fold, while the $S_{0.5}$ is only modestly changed. The results with the I415M substitution are much more drastic: a 100-fold decrease in k_{cat} and an even larger decrease in the terms analogous to V/K compared to WT. The conclusion from this experiment is that for each enzyme an optimum substituent had evolved for this pivotal position, and the bulky substituent with the best fit at position 415 is worth at least 1.4−1.5 kcal/mol in activation energy (transition-state stabilization). The pH dependence of the kinetic parameters for the I415L variant is similar to that exhibited by the WT PDC.

Substrate Inhibition in the Variants. A very noticeable phenomenon in most of the variant PDCs, and less prominent in the WT, is the presence of strong substrate inhibition. While in the WT this inhibition is more pronounced at lower pH values, in several variants there is substrate inhibition apparent in the entire pH range studied. A typical example shown in Figure 3 contrasts the Michaelis−Menten plots of the WT and the I415M variant at pH 7.0. Some of the K_is for pyruvate are in the 20−40 mM range. The behavior of

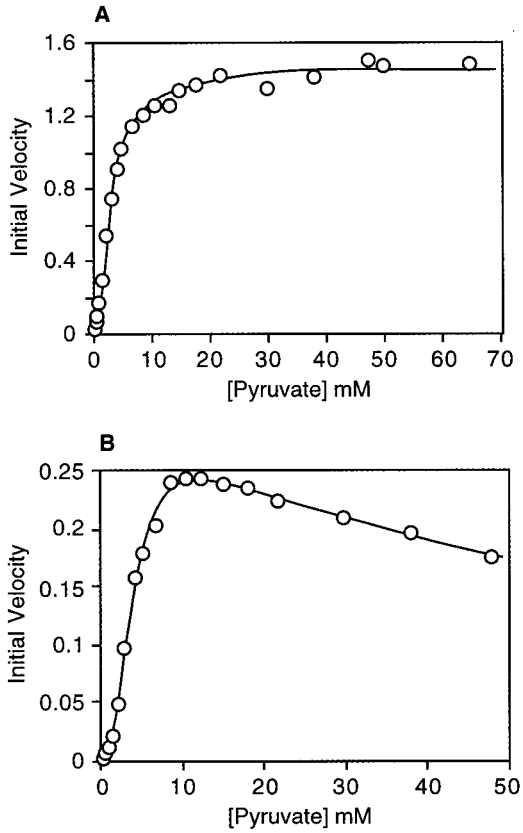

FIGURE 3: Effects of substrate activation and inhibition on (A) wild-type and (B) I415M variant PDC. pH was maintained at 7.0 for both variants, and experiments were carried out at 25 °C.

the k_{cat}−pH and K_i−pH plots shows an interesting parallel. For example, the lower k_{cat} in the acidic range of the pH profile exhibits greater substrate inhibition, while the variants with the lowest k_{cat} values also experience the greatest substrate inhibition.

Computational Studies on the Effects of I415 Substitutions

Computational studies were carried out to explore (a) the effect of the size of the substituent at position 415 on ThDP conformation and (b) whether isoleucine at position 415 on PDC is selected randomly from among bulky side chains or is the optimal choice for this enzyme. The molecular mechanics calculations were performed to estimate the conformational preferences of the thiazolium and 4′-iminopyrimidine rings with respect to the bridging methylene group of the bound ThDP. The definition of the bonds around which the conformational searches were carried out

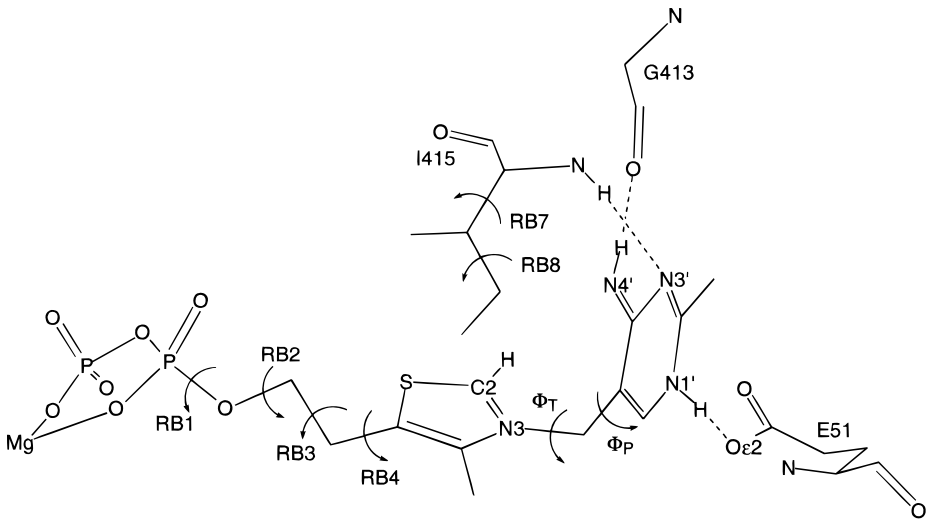

Rotatable Bond	RB1	RB2	RB3	RB4	Φ_T	Φ_P	RB7	RB8
Ref. Value	194.7	190.9	175.3	122.4	97.7	-66.2	69.8	163.2
Range	160-240	120-230	120-220	90-200	60-120	-90 to -30	30-90	90-190
Increment	5	5	5	5	2	2	10	10

FIGURE 4: Definition of rotatable bonds used in the computional studies.

Table 3: Calculated Torsional Angles and Nonbonding Distances for ThDP for WT and I415V, I415A, and I415G PDC Variants[a]

protein		RB1	RB2	RB3	RB4	Φ_T	Φ_P	RB7	RB8	I415NH−N3′	N1′H−E51Oϵ2	N4′H−G413O	N4′−C2H
X-ray[b]		190	192	180	122	96	−75	74	163	2.20	1.83	1.72	2.88
WT	mean[c]	190	190	182	124	94	−68	59	147	2.24	1.87	1.89	2.75
	SD[d]	12.1	11.3	11.6	13.4	7.7	6.4	9.1	16.8	0.21	0.20	0.19	0.23
	high[e]	240	226	210	172	120	−44	80	183	2.98	2.63	2.73	3.48
	low[f]	165	151	125	92	72	−84	50	113	1.58	1.48	1.48	2.23
	min E[g]	195	196	180	117	92	−64	60	153	2.28	1.78	1.83	2.68
I415V	mean	192	184	178	128	95	−68	65		2.18	1.82	1.85	2.77
	SD	12.3	13.6	12.6	14.6	8.9	6.1	9.2		0.22	0.19	0.17	0.27
	high	235	226	210	177	120	−44	80		2.93	2.53	2.58	3.48
	low	165	136	130	92	74	−82	50		1.63	1.48	1.48	2.23
	min E	195	191	180	122	90	−64	60		2.23	1.58	1.88	2.58
I415A	mean	190	183	179	127	98	−63			2.05	1.88	1.98	2.86
	SD	14.6	15.7	15.5	16.6	11.0	11.2			0.24	0.24	0.29	0.32
	high	240	226	215	197	120	−63			2.98	2.83	3.23	3.58
	low	165	121	120	92	68	−84			1.53	1.48	1.48	2.23
	min E	195	191	180	117	94	−68			2.03	1.88	1.78	2.72
I415G	mean	190	183	179	127	98	−62			2.05	1.89	2.00	2.87
	SD	14.6	15.6	15.5	16.6	11.0	11.8			0.24	0.24	0.33	0.33
	high	240	226	215	197	120	−30			2.98	2.83	3.68	3.63
	low	165	121	120	92	62	−84			1.53	1.48	1.47	2.23
	min E	195	191	180	117	94	−68			2.03	1.88	1.78	2.73

[a] See Figure 4 for definition of rotatable bonds (RB) and nonbonding distances. [b] X-ray crystal structure values for the ThDP in one of the unique molecules in the unit cell. [c] Arithmetic mean. [d] Standard deviation. [e] Highest value found for RBs and distances. [f] Lowest value found for RBs and distances; the high and low values define the range of allowable torsional angles and distances within 20 kcal/mol of the global minimum. [g] RBs and distances for the lowest energy conformation.

is presented in Figure 4. Initial searches were carried out with 10° increments along each of the rotatable bonds over a 360° range. Subsequent searches were confined to a narrower range of torsional angles with a finer grid (see Figure 4), identifying conformers within 20 kcal/mol of the global minimum energy conformer. The results for the WT and I415V, I415A, and I415G variant PDCs are presented in Table 3.

The standard deviations are quite informative as a measure of conformational flexibility. Not surprisingly, the smaller the substituent at position 415, the greater the flexibility of ThDP. Also, rotation is more restricted for Φ_P than for Φ_T. Rotation around the C5−C5α bond is less restricted than around the C5α−C5β bond.

The hydrogen-bond distance from the G413 carbonyl oxygen to the 4′-imino hydrogen and from E51 to N1′ (both

Table 4: Calculated Torsional Angles and Nonbonding Distances for 2-(2-Lactyl)-ThDP in WT and PDC Variants[a]

protein		RB1	RB2	RB3	RB4	Φ_T	Φ_P	RB7	RB8	I415NH−N3′	N1′H−E51Oϵ2	N4′H−G413O	N4′−C2α
WT	mean[b]	194	177	173	130	101	−61	64	151	2.30	1.86	1.83	3.28
	SD[c]	12.4	8.0	13.6	9.6	3.8	6.2	8.6	12.3	0.23	0.18	0.16	0.14
	high[d]	240	196	207	165	107	−39	80	183	2.98	2.58	2.48	3.58
	low[e]	164	151	127	106	85	−73	50	133	1.58	1.48	1.48	2.83
	min E[f]	189	186	182	121	97	−57	60	153	2.13	1.88	1.78	3.13
I415V	mean	195	174	171	132	102	−62	66		2.30	1.87	1.81	3.30
	SD	13.2	9.2	13.8	11.3	3.7	6.2	8.9		0.25	0.20	0.17	0.13
	high	239	196	207	171	107	−39	80		2.98	2.53	2.43	3.58
	low	164	136	127	106	87	−73	50		1.59	1.47	1.46	2.85
	min E	194	176	172	131	101	−59	60		2.53	1.80	1.73	3.28
I415A	mean	193	178	176	128	100	−57			2.14	1.88	1.93	3.27
	SD	15.0	9.9	16.3	11.7	5.1	9.5			0.28	0.20	0.23	0.17
	high	239	201	212	176	107	−31			2.93	2.63	2.93	3.73
	low	164	136	127	96	83	−73			1.58	1.48	1.48	2.83
	min E	184	186	187	121	97	−53			2.03	1.88	1.88	3.13
I415G	mean	192	178	176	128	100	−56			2.14	1.88	1.93	3.27
	SD	15.0	9.9	16.3	11.6	5.1	9.5			0.28	0.20	0.24	0.17
	high	239	201	212	176	107	−31			2.93	2.63	3.08	3.78
	low	164	136	127	96	83	−73			1.58	1.48	1.48	2.83
	min E	184	186	187	121	97	−53			2.03	1.88	1.88	3.13

[a] See Figure 4 for definition of rotatable bonds (RB) and nonbonding distances. [b] Arithmetic mean. [c] Standard deviation. [d] Highest value found for RBs and distances. [e] Lowest value found for RBs and distances; the high and low values define the range of allowable torsional angles and distances within 20 kcal/mol of the global minimum. [f] RBs and distances for the lowest energy conformation.

of these hydrogen bonds are conserved in PDC, TK, and POX and presumably in all ThDP enzymes) is satisfactory in all ranges calculated, simply affirming that the potential function does not allow these hydrogen bonds to be broken during the conformational search for WT and I415V.

The key distance between the N4′ and C2 atoms (the ones participating in proton transfer, should the imino tautomeric form of the N1′-protonated ThDP serve as the base responsible for ionizing C2H for the catalytic cycle) was found to increase progressively in going from WT to the I415V to the I415T variant, an increase that may account for the large kinetic differences.

The results of the conformational searches with the C2-bound pyruvate, i.e., a transition-state model, are presented in Table 4. Tables 3 and 4 report data for the 4′-imino tautomer. Stereoscopic views of the lowest energy conformers for WT and I415G in the absence and presence of covalently bound pyruvate are shown in Figure 5.

For comparison, calculations were also carried out for the 4′-amino tautomer of ThDP in the absence of bound substrate, as shown in Table 5. No such calculations were carried out in the presence of covalently bound pyruvate; there was too much steric hindrance apparent. One can conclude with confidence that in the transition-state-like tetrahedral adduct of PDC (LThDP) the coenzyme needs to be in the imino tautomeric form.

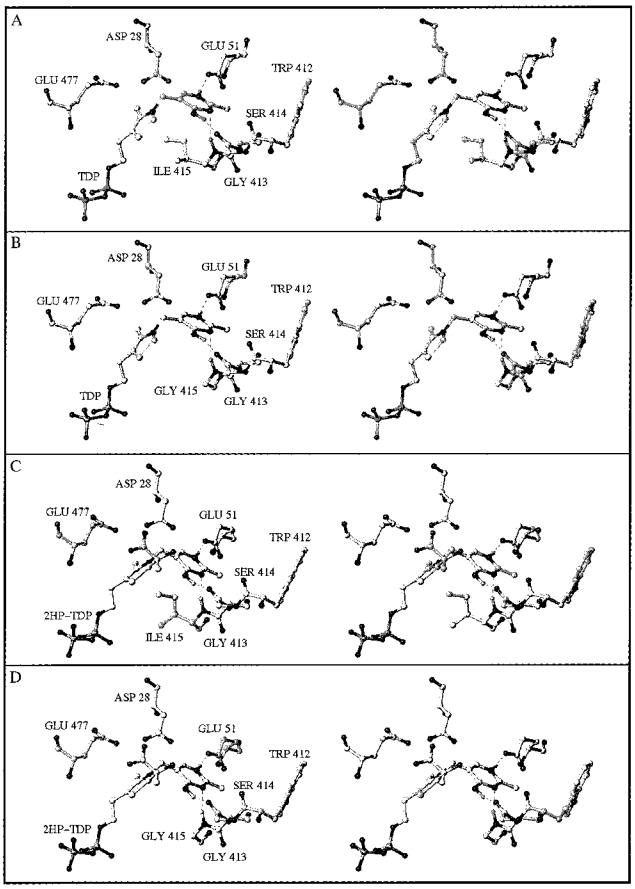

FIGURE 5: Stereoscopic views of minimized structures. (A) WT PDC; (B) I415G PDC; (C) WT with covalently bound pyruvate; (D) I415G PDC with covalently bound pyruvate.

DISCUSSION

Computational Studies

Why Isoleucine Rather than a Smaller Side Chain Is Found at Position 415. The results indicated that the optimal values of the conformational angles for the WT PDC and its I415V variant are very similar to those reported in the X-ray structure. Examination of the second pair, I415A and I415G, revealed that they have similar standard deviations for the conformational parameters, larger than the values obtained for WT and I415V variants. Importantly, the C2−N4′ distance was found to be inversely related to the size of the side chain at position 415, approximately 0.2 Å larger for the I415G and I415A variants. From the trends one can conclude that a side chain larger than Thr (data not shown)

Table 5: Calculation of Conformational Preferences for the 4′-Amino Tautomer of ThDP[a]

protein		RB1	RB2	RB3	RB4	Φ_T	Φ_P	RB7	RB8	I415NH−N3′	N1′H−E51Oϵ2	N4′H−G413O	N4′−C2	N4′−C2H
WT	mean[b]	185	194	187	116	98.8	−76.6	60.4	150	2.22	2.26	1.95		2.97
	SD[c]	10.0	9.0	8.6	9.8	4.9	3.7	9.8	16.7	0.21	0.11	0.24		0.12
	high[d]	229	221	205	152	118	−54.2	79.8	183	2.93	2.73	2.78		3.43
	low[e]	164	161	140	92.4	83.7	−86.2	49.8	113	1.58	2.13	1.48		2.68
	min E[f]	190	191	180	117	99.7	−76.6	59.8	143	2.08	2.18	1.78	3.42	2.98
I415G	mean	187	184	180	122	103	−70.4			2.05	2.29	2.04		3.08
	SD	13.0	16.7	14.4	14.8	8.4	12.6			0.25	0.14	0.40		0.22
	high	234	221	205	187	120	−30.2			2.93	2.93	3.68		3.63
	low	165	121	125	92.4	83.7	−86.2			1.53	2.13	1.48		2.68
	min E	185	191	185	117	102	−74.2			2.08	2.13	1.83	3.40	3.03

[a] See Figure 4 for definition of rotatable bonds (RB) and nonbonding distances. [b] Arithmetic mean. [c] Standard deviation. [d] Highest value found for RBs and distances. [e] Lowest value found for RBs and distances; the high and low values define the range of allowable torsional angles and distances within 20 kcal/mol of the global minimum. [f] RBs and distances for the lowest energy conformation.

is required to reduce the conformational flexibility and to maintain the optimal V conformation, along with the shorter C2−N4′ distance for optimal proton transfer between C2 and the N4′-imino nitrogen. The additional methyl group in isoleucine vs valine is useful to increase the hydrophobicity at the active site, thereby to reduce the local dielectric constant, in turn reducing the activation energy for the various reactions, including decarboxylation of LThDP (*26*, *27*) and perhaps decrease the pK_a of the C2−H. Replacing a hydrogen by a methyl group, via its hydrophobic effect, could stabilize the transition states by as much as 0.6−0.8 kcal/mol (*28*).

The model indicates that there is a strong van der Waals interaction between the C4-methyl group of ThDP and the γ-methyl of I415 (3.3 kcal/mol according to the calculations), an interaction that is absent in the I415V variant. On the basis of this estimate, we suggest that this additional CH_3 group has evolved not only to optimize the hydrophobicity of the environment but also to enhance the binding of the cofactor to the protein, as well as to further reduce the flexibility around rotatable bonds in the cofactor.

The computational studies lead to the following conclusions:

(1) Hydrogen bonds between PDC and 4′-iminopyrimidine of ThDP are weakened by reduction in the size of the side chain at position 415.

(2) In turn, as the size of side chain 415 is decreased, the N4′···C2 distance is increased, i.e., rotation around the Φ_T and Φ_P angles is less restricted. The 3.2 ± 0.23 Å calculated for the N4′−C2 distance is appropriate for direct proton transfer for step k_1 in Scheme 1.

(3) Val imposes very similar steric constraints as Ile.

(4) With a smaller side chain at position 415 (serine, alanine, or glycine), two conformations around the bridging methylene carbon are possible via a 180° flip of the thiazolium ring. Within 11 kcal/mol of the global minimum, the I415A and I415G variants can assume a conformation characterized by the same Φ_P angle but a Φ_T angle that is 180° rotated ($\Phi_T = -82.3°$, $\Phi_P = -112.5°$, and RB4 = 254°) compared to the conformation of the WT PDC. Within 15 kcal/mol of the global minimum, the conserved hydrogen bonds are severed for substituents smaller than Val, resulting in conformations in which the 4′-iminopyrimidine is no longer bound as found in the X-ray structure of WT PDC. On the basis of this estimate, we conclude that the cumulative binding energy of the three conserved hydrogen bonds is worth less than 15 kcal/mol according to the potential function employed.

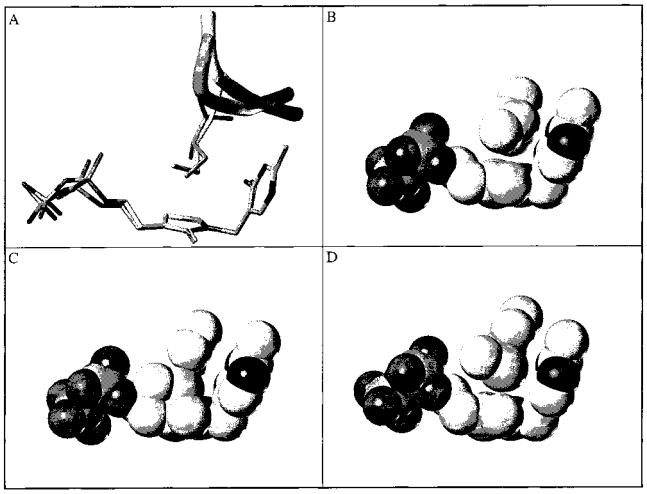

FIGURE 6: (A) Superposition of I415 and ThDP on PDC with M422 and ThDP in POX. The ThDP molecules on the two enzymes are superimposed. (B) Fit of I415 and ThDP on PDC. (C) Attempted fit of M415 and ThDP on PDC. (D) Fit of M422 and ThDP on POX.

(5) The size of the Ile at position 415 precludes any conformation other than that found in the X-ray structure within the 20 kcal/mol window.

Ile at Position 415 Cannot Be Replaced by Residues Found at the Corresponding Sites in Other ThDP Enzymes. A question also examined by experimentation is why nature selected different hydrophobic groups for the position corresponding to 415 in PDC in different ThDP enzymes, Met422 for POX and Leu118 for TK. Superposition of the ThDP coordinates of POX and PDC (Figure 6) revealed that the Cα backbone is pushed back as much as 1.1 Å in the case of POX to accommodate Met (a longer side chain residue than Ile) at the pivotal position. For each enzyme, the bulky amino acid that best fits the backbone appears to have evolved.

Need for, and Consequences of, the V Conformation. It is important to emphasize that *all* variants are predicted to have the ability to achieve the V conformation found in the WT PDC, and diminishing the size of the 415 substituent does not change the fundamental attributes of the V conformation. The three hydrogen bonds conserved at the 4′-aminopyrimidine ring, as well as the Mg(II)−diphosphate

binding site hold the coenzyme already constrained to a near V conformation. The bulky group does add further catalytic efficiency over Ala or even Val, but in its absence the enzyme is still very much an excellent catalyst compared to thiamin as a model for such reactions. As summarized in ref 20, WT PDC enhances the rate of the reaction by a factor of 10^{12} compared to a similar reaction catalyzed by ThDP alone. It appears that the V conformation and the pivotal Ile at position 415 were selected for several reasons: (1) To bring into proximity the N4′ and C2 atoms, probably to enable facile proton transfer to initiate the catalytic cycle; (2) to reduce the conformational flexibility, i.e., freeze out the reactive conformation; and (3) possibly, to avoid collapse of the conformer to tricyclic ThDP (that would result from addition of the 4′-imino nitrogen to the thiazolium C2 atom), an inactive form of the coenzyme. This tricyclic form of thiamin diphosphate with a covalent bond between C2 and N4′ easily fits into the binding pocket of ThDP with either Ala or Gly present at position 415. The fact that the V conformation is universally observed so far suggests that the first reason is most crucial, otherwise, why enforce a conformation that in the absence of enzyme is energetically less favorable? The third suggestion is a consequence of the rich and diverse chemical reactivity of ThDP. Many such reactions probably have no biochemical relevance. On the other hand, these enzymes most likely evolved to avoid potential side reactions; in this case formation of the tricyclic form would render the coenzyme inactive for catalysis if, as widely believed, the Breslow chemistry (*23*) developed for models is the appropriate one for these enzymes.

A more subtle consequence of the V conformation was also revealed: once the proton is transferred to the imino nitrogen, the hydrogen bond between E51 and N1′ is weakened, resulting in a somewhat more relaxed V conformer but with its fundamentals still preserved.

Relative Effects of Substitution at Position 415 on Ground-State and Reactant-State Conformations. The *S* configuration of LThDP is the one that best fits the active center, as also reported by Lobell and Crout (*29*), bringing the side-chain C2α−OH into close proximity of the N4′ atom. The *R* configuration is disfavored because of the larger steric effect of the CH_3 group compared to OH. The flexibility according to the standard deviation values is nearly the same in the pyruvate−ThDP adduct (LThDP, our model for the decarboxylation transition state) *for any substituent at position 415*. The flexibility around various bonds is always more restricted in the LThDP analogues than in the case of unsubstituted ThDP. The reduction in flexibility in going from the ground-state structure to the LThDP or transition-state-like structures is less with a bulky substituent at position 415 (isoleucine in the WT PDC) than with a small substituent such as alanine. In other words, the rotational (conformational) entropy in the ground state is more negative for Ile (the larger substituent) than for a smaller substituent. This, in turn, suggests that there is less of an unfavorable entropy contribution $\Delta S^{\ddagger}$ to the $\Delta G^{\ddagger}$ for the larger substituent at position 415 in WT, in turn leading to faster rates, in accord with the Jencks hypothesis (*30*).

Implications for Catalysis from Kinetic Data

Our current working hypothesis for the mechanism is shown in Scheme 2. In the upper left-hand corner of the scheme is shown an approximate version of the scheme presented by Schowen and collaborators (*20*). There are a number of events one must keep in mind to account for the observations. Addition of the first substrate is presumably to the regulatory site—PDC from yeast is known to be hysteretic (*31*, *32*) and there is accumulating evidence that cysteine 221 is the side chain that triggers this hysteretic behavior in the presence of pyruvate (*12*−*16*). There is also accumulating evidence going back more than 20 years that the 4′-amino group is an active participant in the mechanism. To account for its reactivity, it was shown in models that protonation of the N1′ atom would convert the amino group to its conjugate base (the imino tautomer) with a pK_a of 12−12.6 (*24*, *33*, *34*). As shown in the upper right-hand side of Scheme 2, protonation at N1′ sets up the tautomeric equilibrium between the 4′-amino and the 1′-H, 4′-imino tautomer. The computational studies, in conjunction with the experimental data (*24*), suggest that the amino group would be coplanar with the pyrimidine ring and strongly endorse the idea that the catalytically active form is the imino tautomer. We prefer to regard the Glu51−HN1′−HN4′ relay as a single catalytic dyad whose function is to extract the proton from C2 to generate the ylide/carbene (the two extreme resonance structures).

Under Addition of Pyruvate to ThDP in Scheme 2, we start with the E·S* complex, the activated form of the enzyme. Three mechanisms can be written for this step: (a) the PDC-bound ThDP exists as the conjugate base (ylide/carbene); (b) the ylide is formed in a distinct step but is rapidly trapped by the substrate, and (c) there is a synchronous proton transfer and C−C bond-making event to form the LThDP. While one former hydrogen exchange study suggested the concerted pathway (*35*), a more recent paper (*36*) concluded that (a) in the absence of substrate, but also in the activated form of the enzyme, the thiazolium ring exists in its undissociated form and (b) proton transfer may be rate-limiting in the absence of activation but is much faster than the turnover number in the activated form of PDC. For either mechanism, we suggest that the 4′-imino nitrogen shuttles the proton from C2H to the incipient alkoxide to neutralize the negative charge and to alleviate steric crowding. There may also be a need to neutralize the second negative charge, the one on the carboxylate group of the substrate, a function that could be served by a hydrogen bond with the D28 carboxylic acid group according to molecular modeling.

Continuing with our minimalist view, we speculate that the decarboxylation step itself proceeds with relatively modest assistance from the protein, except for an environmental effect, a low effective dielectric constant at the active center created in part by I415. Catalysis is required for the product release steps. First, the enamine/C2α carbanion needs to be protonated. This could be accomplished by any potential acid catalyst on PDC, such as D28 or E477, or the water solvent. Model studies for this step for benzoylformate decarboxylase (the methyl of pyruvate in PDC being replaced by a phenyl group) have suggested that this proton transfer does require assistance by a general acid group on the enzyme (*37*, *38*). Finally, in a role mirroring the catalysis for substrate addition, the 4′-imino group would participate in the release of acetaldehyde. We believe that the minimalist view is worthy of consideration in view of the lack of conservation of acid−base residues in PDC from yeast

and benzoylformate decarboxylase (BFD), enzymes with virtually the same function. For example, D28 and E477 appear to have no counterparts in BFD, therefore the proton-transfer and/or hydrogen-bonding mechanisms leading to the lowering of the kinetic barriers may not have been conserved among these enzymes.

A plausible model to account for the bell-shaped k_{cat}−pH, k_{cat}/B−pH, and k_{cat}/A−pH (and $k_{cat}/S_{0.5}$−pH) profiles in Figure S1 requires the participation of at least one ionizable side chain in the conjugate acid and one in the conjugate base form. The first three kinetic terms represent rate constants zero, first, and second order in substrate concentration (as derived in ref 20, the constants *A* and *B* are analogous to K_m, which due to the hysteretic behavior is replaced by $S_{0.5}$) and can also be thought of as rate-limiting events at high ($[S] \gg S_{0.5}$), intermediate, and low ($[S] \ll S_{0.5}$) substrate concentrations. In the Hill formulation, k_{cat} and $k_{cat}/S_{0.5}$ should be considered. Elsewhere, we will show that modification of any of the potential acid−base catalysts at the active center [E51 (Y. Gao and J. Wang, unpublished results); D28, H114, H115, and E477 (F. Guo and J. Wang, unpublished results)] leads to changes in k_{cat} and its pH dependence; i.e., they are all involved in catalysis. While the involvement of E51 is mediated by the 4′-iminopyrimidine (the latter shields E51 from the substrate), the other four residues could participate in the reactions directly. The residue I415 introduces no additional charge into the active center, hence it cannot be directly involved in proton transfers. On the basis of the computational study, I415 has a significant effect on the mobility of ThDP at the active center, very likely affecting the alignment of the hydrogen bonds between E51 and the N1′−H, the main-chain NH of I415 and N3′, and the C═O of S413 and N4′−H of the 4′-iminopyrimidine (and perhaps of the other acid−base groups), thereby stabilizing a variety of transition states along the reaction pathway.

Interpretation of Changes in k_{cat}. According to the formulation of eq 1, k_{cat} encompasses transition states starting with decarboxylation and including product release. Plausible candidates based on modeling would be D28-COOH to facilitate decarboxylation by neutralizing the negative charge at the carboxylate, the D28-COOH or E477-COOH to protonate the enamine, and the 4′-imino nitrogen to assist with acetaldehyde release. A water molecule is found at D28, which would be displaced by the bound substrate but perhaps would supply the required proton (*2*). According to the crystal structure currently in hand, residues H114 and H115 are too far from the active center to be considered. However, as pointed out in a recent report of variants at the corresponding positions in PDC from *Zymomonas mobilis*, these conserved histidines are located on a flexible loop, which could move closer to the active center during the reaction (*39*). The magnitude of the $^{13}CO_2/^{12}CO_2$ kinetic isotope effect on k_{cat} was attributed to similar barriers for decarboxylation and product release (*20*), with

$$1/k_{cat} = 1/k_{decarboxylation} + 1/k_{enamine\ protonation} + 1/k_{product\ release} \quad (2)$$

A comparison of the pH dependence of k_{cat} for WT and the I415V and I415T variants suggests that the side chain(s) responsible for the acid limb of the profile has moved with respect to LThDP, decreasing the rate constant and the conjugate acidity of the species responsible for catalysis. A plausible candidate for this event is the 4′-imino nitrogen assisting with acetaldehyde release. Proton transfers appear to be part of rate limitation not only in WT but also in the I415V and I415T variants and the rate-limiting steps could indeed be the same for all three enzyme variants. Were the barriers similar for all three steps in eq 2, a possible explanation is synchronous enamine protonation by D28 or E477, or a nearby water molecule, and product release by the 4′-imino group. The rate-limiting steps would be expected to change with pH. For example, the decreasing rate of the reaction at low pH could be due to rate-limiting acetaldehyde release. The alkaline p*K* shift experienced with the less hydrophobic side chains of V and T (Table 2) could be due to lower acidity of the alcohol (the alkoxide is a zwitterion) with higher effective dielectric constant. In the case of the I415M and I415A variants, the major perturbation in the active center is reflected in lower sensitivity to pH effects; i.e., proton transfers are no longer as dominant in rate limitation.

Interpretation of Changes in k_{cat}/A and k_{cat}/B. The term k_{cat}/A varies with the second power of substrate concentration and includes transition states starting with the addition of the first pyruvate, presumably at the regulatory site C221 and culminating with decarboxylation. In the case of WT enzyme, the rather narrow pH profile suggests that there are at least two charged residues (pK_as 5.3 and 6.4) modulating this curve and involved in the rate-limiting steps. The similarity of the pK_as controlling the acid limb of the k_{cat}/A−pH and $k_{cat}/S_{0.5}$−pH plots for WT and *all I415 variants* (Table 2), and the absence of this downturn with decreasing pH in the C221S variant (*15*) prompts us to conclude that C221 contributes substantially to this behavior. On the basis of the pH dependence of the Hill coefficients (*15*) and earlier Fourier transform infrared (FTIR) and isoelectric focusing studies (*14*), we concluded that C221 has a pK_a of 5.2. While the k_{cat}/A−pH curves are not fully defined for the I415V and I415T variants, the $k_{cat}/S_{0.5}$−pH curves are clearly bell-shaped, as they are for the WT and the I415M and I415A variants.

The term k_{cat}/B varies with the first order of substrate concentration and it includes transition states starting with the activated SE* complex and culminating in decarboxylation. It includes formation of LThDP (both proton transfer from the thiazolium and C−C bond formation) and its decarboxylation. The k_{cat}/B values of the I415 variants are lower than that of the WT, indicating that the rate-limiting step for this sequence is also affected by substitutions at position 415. In the I415V and I415T variants, k_{cat}/B is pH-dependent with slight alkaline shifts of the pK_as compared with WT, again suggestive of the involvement of hydrogen-bonding and/or proton-transfer reactions in rate limitation. In the case of the I415M above pH 5.5 and I415A above pH 6.0, the rates of product formation are no longer linear in substrate concentration. The similarity of the shape of the k_{cat}/B−pH and the $k_{cat}/S_{0.5}$−pH profiles for each I415 variant suggests that the information resulting from binding the regulatory substrate molecule at C221 arrives at the active center essentially unaltered by the I415 substitutions and the rate-limiting step(s) also remain the same. According to our early $^{13}CO_2/^{12}CO_2$ kinetic isotope effects on decarboxylation

measured under $V/S_{0.5}$ conditions (*40*), and those on *V*/*A* and *V*/*B* (*20*), decarboxylation is no more than 10−20% of rate limitation in this case. We therefore suggest that the pH dependence pertains to formation of the covalent LThDP adduct, tentatively the E51−iminopyrimidine dyad being responsible for the acid limb, and perhaps D28 for the alkaline limb of the pH profile (it is difficult at the present to rule out E477, H114, and H115). The observation that decarboxylation is more rate-limiting under these conditions at lower pH (*40*) also suggests that the relative barrier heights for LThDP formation and decarboxylation vary with pH. The similarity of the pK_as controlling the acid limb of the k_{cat}−pH and k_{cat}/B−pH profiles suggests that the Glu51−4′-iminopyrimidine dyad participates in the rate-limiting steps once the fully substrate-activated enzyme ES* is formed (at intermediate and high substrate concentrations).

Substrate Inhibition Is Prominent in the PDC Variants. The pronounced substrate inhibition observed in the WT appears to be modulated by a side chain with a pK_a of 5.4 in its conjugate acid form; the K_i is smaller (inhibition is stronger) at lower pH. The I415V and I415T variants exhibit an alkaline shift compared to the WT, as also observed for the k_{cat} values. The I415M and I415A variants also exhibit strong but pH-independent substrate inhibition. The values of K_i and k_{cat} appear to be modulated by side chains with very similar pK_as, suggesting that the two phenomena are coupled and that the same side chain may be responsible for both turnover and substrate inhibition. Substrate inhibition is more prominent in the variants than in the WT PDC. A possible candidate for this inhibition is the known acetoin- and acetolactate-forming reaction, while the appearance of this inhibition must also signal the reduction of a negative field (or increasing positive field) at the active center to accommodate the additional negative charge.

Effects of Substitutions at Position 415 on Substrate Activation. According to the Hill coefficients, the positive homotropic effect of pyruvate is not abolished by any of the substitutions. It has been demonstrated that C221 on the β domain acts as the trigger for substrate activation (*12*−*16*) and the information is then transmitted to ThDP located more than 20 Å away between the α and γ domains. The pathway identified so far suggests that on attachment of the substrate to C221 either noncovalently, or covalently via a hemithioketal, the information is transferred from C221 to H92 of the α domain, resulting in dislocation of H92. This distortion is sensed by the adjacent E91, which in turn makes a hydrogen bond to the main-chain NH of W412, part of a five-residue loop (411−415) that terminates in I415. On the basis of our evidence presented here, it appears that the information is likely transmitted to G413, whose carbonyl oxygen is hydrogen-bonded to the N4′H of the coenzyme (one of three conserved hydrogen bonds holding the 4′-aminopyrimidine ring of the coenzyme in place), *but I415 is not involved in the substrate activation pathway*.

Finally, the results of this study suggest that the positions equivalent to I415 on ThDP enzymes also provide an interesting system with which to test current theories of enzyme action. In particular, whether enzymes reduce kinetic barriers by ground-state destabilization or transition-state stabilization and whether the entropic or enthalpic contributions to the free energy of activation are most prominent continues to be a source of intense experimentation and computational studies (*41*). Since X-ray structures are not yet available for any reaction intermediates of PDC, we cannot unequivocally state what happens in the transition-state-like complexes. However, our modeling of the LThDP−PDC complex certainly suggests that Ile at position 415 provides an entropic contribution that raises the free energy of the S−E−S* covalent complex to a higher level (relative to E−S* + S) than would a smaller substituent (G or A) at the same position, thereby reducing the barrier for the decarboxylation step in the wild-type PDC.

ACKNOWLEDGMENT

We are grateful to Dr. Phil Huskey for his help with some of the kinetic analysis and useful discussions of the data.

SUPPORTING INFORMATION AVAILABLE

Figures S1A−E and Tables S1−S5, showing the results of steady-state kinetic studies at different pH values for wild-type PDC and the I415V, I415T, I415A, and I415M variant PDCs (10 pages). Ordering information is given on any current masthead page.

REFERENCES

1. Dyda, F., Furey, W., Swaminathan, S., Sax, M., Farrenkopf, B., and Jordan, F. (1993) *Biochemistry 32*, 6165−6170.
2. Arjunan, D., Umland, T., Dyda, F., Swaminathan, S., Furey, W., Sax, M., B. Farrenkopf, B., Gao, Y., Zhang, D., and Jordan, F. (1996) *J. Mol. Biol. 256*, 590−600.
3. Muller, Y. A., and Schulz, G. E. (1993) *Science 259*, 965−967.
4. Lindquist, Y., Schneider, G., Ermler, U., Sundstrom, M. (1992) *EMBO J. 11*, 3273−3279.
5. Shin, W., Pletcher, J., Blank, G., and Sax, M. (1977) *J. Am. Chem. Soc. 99*, 3491−3499.
6. Shin, W., Pletcher, J., Sax, M., and Blank, G. (1979) *J. Am. Chem. Soc. 101*, 2462−2469.
7. Shin, W., and Kim, Y. C. (1986) *J. Am. Chem. Soc. 108*, 7078−7082.
8. Power, L., Pletcher, J., and Sax, M. (1970) *Acta Crystallogr. B 26*, 143−148.
9. Jordan, F. (1974) *J. Am. Chem. Soc. 96*, 3623−3629.
10. Jordan, F. (1976) *J. Am. Chem. Soc. 98*, 808−813.
11. Shin, W., Oh, D.-G., Chae, C.-H., and Yoon, T.-S. (1993) *J. Am. Chem. Soc. 115*, 12238−12250.
12. Zeng, X., Farrenkopf, B., Hohmann, S., Dyda, F., Furey, W., and Jordan, F. (1993) *Biochemistry 32*, 2704−2709.
13. Baburina, I., Gao, Y., Hu, Z., Jordan, F., Hohmann, S., and Furey, W. (1994) *Biochemistry 33*, 5630−5635.
14. Baburina, I., Moore, D. J., Volkov, A., Kahyaoglu, A., Jordan, F., and Mendselsohn, R. (1996) *Biochemistry 35*, 10249−10255.
15. Baburina, I., Li, H., Bennion, B., Furey, W., and Jordan, F. (1998) *Biochemistry 37*, 1235−1244.
16. Baburina, I., Dikdan, G., Guo, F., Tous, G. I., Root., B., and Jordan, F. (1998) *Biochemistry 37*, 1245−1255.
17. Sarkar, G., and Sommer, S. (1990) *BioTechniques 8*, 404−07.
18. Bradford, M. (1976) *Anal. Biochem. 72*, 248−254.
19. Holzer, H., Schultz, G., Villar-Palasi, C., and Jutgen-Sell, J. (1956) *Biochem. Z. 327*, 331−344.
20. Alvarez, F. J., Ermer, J., Hübner, G., Schellenberger, A., and Schowen, R. L. (1991) *J. Am. Chem. Soc. 113*, 8402−8409.
21. Dixon, M., and Webb, E. C. (1974) *Enzymes*, 2nd ed., p 116, Longmans, Green, New York.
22. Clark, M., Cramer, R. D., III, and Van Opdenbosch, N. (1989) *J. Comput. Chem. 10*, 982−1012.
23. Breslow, R. (1958) *J. Am. Chem Soc. 80*, 3719−3726.

24. Jordan, F. (1982) *J. Org. Chem. 47*, 2748−2753.
25. Farrenkopf, B., and Jordan, F. (1992) *Protein Expression Purif. 3*, 101−107.
26. Crosby, J., Stone, R., and Lienhard, G. E (1970) *J. Am. Chem. Soc. 92*, 2891−2900.
27. Crosby, J., and Lienhard, G. E (1970) *J. Am. Chem. Soc. 92*, 5707−5716.
28. Tanford, C. (1979) *The hydrophobic effect; formation of micelles and biological membranes*, p 12, John Wiley and Sons, New York.
29. Lobell, M., and Crout, D. H. G. (1996) *J. Am. Chem. Soc. 118*, 1867−1873.
30. Jencks, W. P. (1975) *Adv. Enzymol. Relat. Areas Mol. Biol. 43*, 219−410.
31. Boiteaux, A., and Hess, B (1970) *FEBS Lett. 9*, 293−296.
32. Hübner, G., Weidhase, R., and Schellenberger, A. (1978) *Eur. J. Biochem. 92*, 175−181.
33. Jordan, F., and Mariam, Y. H. (1978) *J. Am. Chem. Soc. 100*, 2534−2541.
34. Jordan, F., Chen, G., Nishikawa, S., and Sundoro-Wu B. (1982) *Ann. N.Y. Acad. Sci. 378*, 14−31.
35. Harris, T. K., and Washabaugh, M. W. (1995) *Biochemistry 34*, 13994−14000.
36. Kern, D., Kern, G., Neef, H., Tittmann, K., Killenberg-Jabs, M., Wikner, C., Schneider, G., and Hübner, G. (1997) *Science 275*, 67−70.
37. Barletta, G., Huskey, W. P., and Jordan, F. (1992) *J. Am. Chem. Soc. 114*, 7607−7608.
38. Barletta, G. L., Huskey, W. P., and Jordan, F. (1997) *J. Am. Chem. Soc. 119*, 2356−2362.
39. Schenk, G., Leeper, F. J., England, R., Nixon, P. F., and Duggleby, R. G. (1997) *Eur. J. Biochem. 248*, 63−71.
40. Jordan, F., Kuo, D. J., and Monse, E. U. (1978) *J. Am. Chem. Soc. 100*, 2872−2878.
41. Lightstone, F. C., and Bruice, T. C. (1997) *J. Am. Chem. Soc. 119*, 9102−9113.

BI9807097